Structural Engineering and Mechanics, *Vol. 71, No. 5 (2019) 469-483*
DOI: https://doi.org/10.12989/sem.2019.71.5.469

Bending analysis of doubly curved FGM sandwich rhombic conoids

Md I. Ansari[1], Ajay Kumar*[2] and Ranja Bandyopadhyaya[2]

[1]*Department of Architecture, Jamia Millia Islamia, New Delhi- 110025, India*
[2]*Department of Civil Engineering, National Institute of Technology Patna, Patna- 800005, India*

(Received February 28, 2019, Revised March 26, 2019, Accepted April 22, 2019)

Abstract. In this paper, an improved mathematical model is presented for the bending analysis of doubly curved functionally graded material (FGM) sandwich rhombic conoids. The mathematical model includes expansion of Taylor's series up to the third degree in thickness coordinate and normal curvatures in in-plane displacement fields. The condition of zero-transverse shear strain at upper and lower surface of rhombic conoids is implemented in the present model. The newly introduced feature in the present mathematical model is the simultaneous inclusion of normal curvatures in deformation field and twist curvature in strain-displacement equations. This unique introduction permits the new 2D mathematical model to solve problems of moderately thick and deep doubly curved FGM sandwich rhombic conoids. The distinguishing feature of present shell from the other shells is that maximum transverse deflection does not occur at its center. The proposed new mathematical model is implemented in finite element code written in FORTRAN. The obtained numerical results are compared with the results available in the literature. Once validated, the current model was employed to solve numerous bending problems by varying different parameters like volume fraction indices, skew angles, boundary conditions, thickness scheme, and several geometric parameters.

Keywords: functionally graded sandwich shell; conoids; finite element method; rhombic shell

1. Introduction

A sandwich-structured composite provides high bending stiffness as compared to the conventional material, that makes it more favourable in lightweight structure. Due to the large jump of material properties at the layer interfaces, the problem of delamination is generally observed in conventional sandwich structures. The concept of FGM is also employed in such sandwich structures to overcome this problem. The FGM is an inhomogeneous material, composed of two (or more) materials, organized with a view to having a smooth gradation in the desired direction. Koizumi (1997) used FGM in advance engineering structures experiencing elevated temperatures. Eslami *et al.* (2005) developed a general solution for the 1-D steady-state mechanical and thermal stresses in an FGM hollow thick sphere. Zenkour and Alghamdi (2008) analysed the functionally graded sandwich plate subjected to a thermal load. Static response of functionally graded cylindrical shells using the element-free kp-Ritz method was analysed by Zhao *et al.* (2009). An elastic solution for a sandwich panel with isotropic skins is presented by Kashtalyan and Menshykova (2009). A numerical 3D thermo-elastic solution for the functionally graded hollow cylindrical shell having piezoelectric layers subjected to asymmetric thermo-electro-mechanical loads has been exhibited by Alashti and khorsand (2011). Higher order shear deformation model having four unknowns is studied for static analysis of functionally graded sandwich plate by Abdelaziz *et al.* (2011). Merdaci *et al.* (2011) proposed two shear deformation theories for the analysis of the static behaviour of FGM sandwich plate. Their theories demonstrated the parabolic distribution of the transverse shear strains. Natarajan and Manickam (2012) considered a realistic variation in displacement along thickness direction in higher order model for the bending and flexure vibration behaviour of FGM sandwich plate. A refined trigonometrical higher-order theory accounting transverse shear and the normal strain were used to discuss the bending behaviour of FGM sandwich plate by Zenkour (2013). Taj *et al.* (2014) have used Reddy's higher order theory by incorporating a C0 FE formulation to study the behaviour of FGM skew shell panel. Bessaim *et al.* (2013) developed five unknown based shear deformation theory for the static analysis of FGM sandwich plate. The stresses in functionally graded doubly curved shells were calculated by incorporating differential quadrature method in the first order shear deformation theory by Tornabene and Viola (2013). An analytical solution is developed by Sayyad and Ghugal (2014) to account the effect of transverse shear and transverse normal for the bending analysis of isotropic, laminated composite and sandwich plates. Viola *et al.* (2014) used unconstrained third-order shear deformation theory for the static analysis of moderately thick functionally graded conical shells. Asemi *et al.* (2014) used classical theory for linear thermoelastic analysis of thick cone. Dai and Dai (2014) developed an analytical solution based upon classical shell theory for FGM cylindrical shell under thermomechanical loading. Ghannad and Gharooni (2014) used FSDT model to calculate stresses and displacement in thick FGM cylinders. Xiang and Liu (2016) used meshless global collocation method with nth-order

*Corresponding author, Ph.D.
E-mail: er.mdirfan2k9@gmail.com

http://www.techno-press.com/journals/sem&subpage=7
ISSN: 1225-4568 (Print), 1598-6217 (Online)

shear deformation theory for the static analysis of FGM sandwich plate. Hadji *et al*. (2016) proposed a new mathematical model based on FSDT for the static and dynamic analysis of FGM plate. Alipour and Shariyat (2017) investigated the free vibration analysis of sandwich plates with isotropic/orthotropic face sheet and different combinations of boundary conditions. Daouadji and Adim (2017) explored the behaviour of FGM sandwich plate using hyperbolic shear and normal deformation theory.

Since casting and fabrication of conoids possessing singly ruled surface is quite easy, hence it is favoured in the construction industry. The advancements in composite technology have made it possible to design a strong and stiff composite has blossomed a new inspiration for researchers to study about conoidal shells. Conoids shells are esthetically appealing, structurally stiff and are used to cover the column-free large area in aircraft hangars, exhibition hall and industrial structures. A comprehensive study of bending response under various types of mechanical load is essential to access the optimal use of rhombic conoids. A combined variational approach was used by Hadid (1964) for the bending response of both simply supported and clamped elastic conoids. In his formulation, he modifies the shell equations (expressed in terms of displacement) in the ordinary differential equation using Kantorovich method. Ghosh and Bandyopadhyay (1990) and Dey *et al*. (1992) used finite element (FE) technique for the bending analysis of doubly curved isotropic shell and analysis of composite conoidal shell structure respectively. Finite difference method was carried out on the conoidal shell by Das and Bandyopadhyay (1993) for both experimental as well as theoretical investigation. Ghosh and Bandyopadhyay (1994) engaged their own formulation to examine the influence of cutouts on static analysis of conoidal shells. The bending analysis of stiffened conoids is studied by Das and Chakravorty (2009) using three noded beam element. Kumari and Chakravorty (2010) used FSDT for the study of bending response of delaminated conoids. The FE method was used by Bakshi and Chakravorty (2014) for the analysis of first ply failure occurs in laminated composite conoidal shell subjected to uniformly distributed loading. The free vibration analysis of rotating CNTRC truncated conical shell are studied by Heydarpour *et al*. (2014) using FSDT. Civalek (2017b, 2017a) is studied the free vibration and buckling behaviour of conical and cylindrical shell composites reinforced with CNT. Malekzadeh Fard and Baghestani (2017) explored the free vibration behavior of moderately thick doubly curved shell based on FSDT with classic boundary conditions. Jooybar *et al*. (2016) presented the vibration analysis of FG-CNTRC truncated conical panel with elastically restraint edges subjected to the thermal environment. Demirbas (2017) developed an elastic theory whereas Demirbas and Apalak (2017) used finite element method for thermal analysis of FGM plate subjected to in-plane constant heat flux.

The literature review reveals that there has not been substantial work regarding the bending analysis of doubly curved FGM sandwich rhombic conoids. Therefore, an attempt has been made in the present paper to study the bending behaviour of FGM sandwich rhombic conoidal shell with the help of a proposed new mathematical model. The FE coding for the present new mathematical model is done by using a C^0 nine noded FE with seven nodal unknowns at each node developed by authors. C^1 continuity requirement associated with the present model is suitably circumvented. The present study facilitates the ease of bending analysis by finite element (FE) modelling, keeping in mind the processing time in computer and simplicity of approach. This study is the first step toward enhancing our understanding of bending problem of FGM sandwich rhombic conoidal shell, hence the present results may serve as a benchmark for future research in this field.

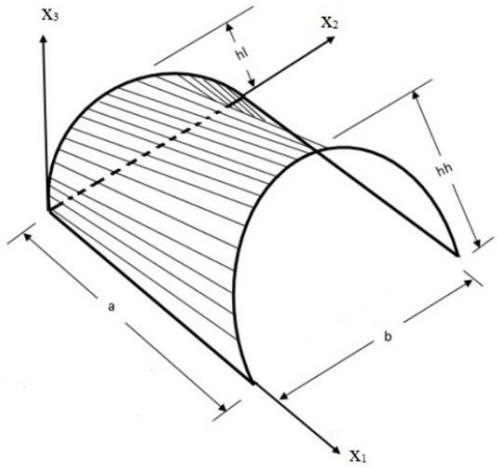

$$x_3 = 4\left[hl + \left(hh - hl\right)\frac{x_1}{a}\right]\left[\frac{x_2}{b} - \frac{x_2^2}{b^2}\right]$$

Fig. 1 Geometry and surface equation of conoidal shell

2. Modelling and effective material properties

2.1 Modelling of FGM rhombic conoidal shell

A single layered FGM conoidal shell of sides a, b and thickness h are depicted in Fig. 1. The upper layer $(x_3 = +h/2)$ of the shell surface is ceramic rich; while the bottom portion $(x_3 = -h/2)$ of the shell surface is metal rich as shown in Fig. 2(a), with a gradation zone having a smooth variation of material properties in between the two surfaces.

Using the power law, the effective properties of the FGM rhombic conoidal shell at any point in thickness coordinate can be stated as

$$P\left(x_3\right) = P_c V_c\left(x_3\right) + P_m V_m\left(x_3\right) \tag{1}$$

$$\text{where } V_c(x_3) = \left(\frac{1}{2} + \frac{x_3}{h}\right)^n, (0 \le n \le \infty) \quad \text{and } V_c\left(x_3\right) + V_m\left(x_3\right) = 1 \tag{2}$$

Once the volume fraction index of material constituents is known, the Young's modulus of the FGM shell at any point 'x_3' can be calculated as per the rule of mixture.

$$E(x_3) = E_c V_c(x_3) + E_m V_m(x_3) \tag{3}$$

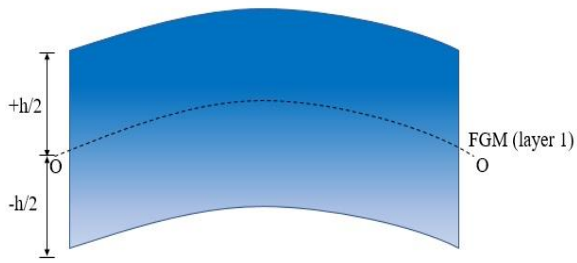

(a) FGM conoidal shell

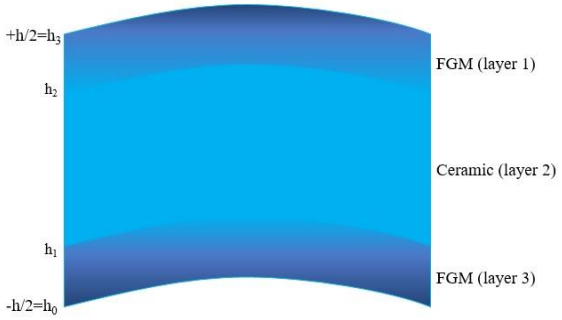

b) FGM Type-I sandwich conoidal shell having homogenous core

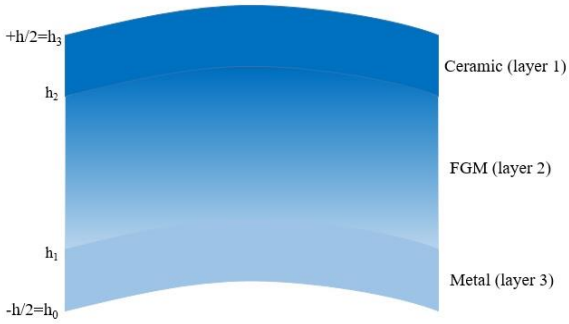

(c) FGM Type-II sandwich conoidal shell having FGM core

Fig. 2 Thickness scheme of FGM conoidal shell and sandwich conoidal shell

Where, E_m and E_c are the material properties of metal and ceramic respectively, V_c and V_m are the volume fraction of ceramic and metallic component respectively and n is the volume-fraction index.

2.2 Modelling of FGM sandwich rhombic conoidal shell Type-I

Fig. 2(b) shows the thickness of the FGM sandwich shell having ceramic rich core portion while the top portion and bottom portion is occupied by FGM. Since the material properties of the rhombic sandwich conoidal shell are different in each layer, the effective material properties as Young's modulus of any layer can be calculated as

$$E(x_3) = E_c V_c^i(x_3) + E_m V_m^i(x_3) \tag{4}$$

where V_c^i and V_m^i is the volume fraction of ceramic and metallic constituents of the *i*th layer, respectively.

The volume fraction of each layer from top to bottom is defined by the following expressions

$$V_c^1 = \left(\frac{x_3 - h_3}{h_2 - h_3}\right)^n, \quad x_3 \in [h_2, h_3] \tag{5}$$

$$V_c^2 = 1, \quad x_3 \in [h_1, h_2] \tag{6}$$

$$V_c^3 = \left(\frac{x_3 - h_0}{h_1 - h_0}\right)^n, \quad x_3 \in [h_0, h_1] \tag{7}$$

The thickness ratio taken for the present study of each layer is 1-0-1, 1-1-1, 1-2-1, 2-1-2 and 2-2-1. For the 1-2-1 FGM conoidal shell, the core layer is made of twice the thickness of the top and bottom layer, i.e. $h_2 = h/4$ and $h_1 = -h/4$. For the thickness ratio 1-1-1, the thickness of the core is same as the top layer and bottom layer, $h_2 = h/6$ and $h_1 = -h/6$. For other thickness ratios, the value of h_1 and h_2 can be calculated same as the above.

2.3 Modelling of FGM sandwich rhombic conoidal shell Type-II

In the second type of FGM sandwich shell shown in Fig. 2 (c), the top and bottom layer of the shell is occupied by ceramic and metal respectively. By using this a sandwich shell with FGM core and isotropic skin having smooth variation across the thickness can be modelled. This type of arrangement of layer gives the minimum stress concentration at the layer interface. The volume fraction of each layer can be expressed by the following expression.

$$V_c^1 = 0, \quad x_3 \in [h_2, h_3] \tag{8}$$

$$V_c^2 = \left(0.5 + \frac{x_3}{h_2 - h_1}\right)^n, \quad x_3 \in [h_1, h_2] \tag{9}$$

$$V_c^3 = 1, \quad x_3 \in [h_0, h_1] \tag{10}$$

The thickness ratio taken for the present study of each layer from top to bottom is 1-8-1. For the thickness ratio 1-8-1, the thickness of core (layer 2) is 8 times the thickness of the top layer, $h_2 = h/16$ and $h_1 = -h/16$.

3. Mathematical formulation of the problem

3.1 Assumed displacement field and strains

To derive the mathematical model, the displacement fields for FGM shell is considered on the basis of the third order shell theory and are as follows:

$$\begin{aligned}
u(x_1, x_2, x_3) &= \left(1 + \frac{x_3}{R_{x_1}}\right) u_0(x_1, x_2) + x_3\, \theta_{x_1}(x_1, x_2) \\
&+ x_3^2\, \xi_{x_1}(x_1, x_2) + x_3^3\, \zeta_{x_1}(x_1, x_2) \\
v(x_1, x_2, x_3) &= \left(1 + \frac{x_3}{R_{x_2}}\right) v_0(x_1, x_2) + x_3\, \theta_{x_2}(x_1, x_2) \\
&+ x_3^2\, \xi_{x_2}(x_1, x_2) + x_3^3\, \zeta_{x_2}(x_1, x_2) \\
w(x_1, x_2, x_3) &= w_0(x_1, x_2)
\end{aligned} \tag{11}$$

where the middle section is taken as reference for material coordinates (x_1, x_2, x_3). u, v, w denoted as the displacements of a point along the (x_1, x_2, x_3) coordinates, u_0, v_0, w_0 are corresponding displacements on the mid-plane. θ_{x_1} and θ_{x_2} are the bending rotations normal to the mid-plane about the x_2 axis and x_1 axis, respectively. The functions $\xi_{x_1}, \xi_{x_2}, \zeta_{x_1}$ and ζ_{x_2} are higher order terms of Taylor's series expansion at the mid-plane of the conoidal shell. By imposing the boundary condition (transverse shear strain at top and bottom = 0) in Eq. (11), the function $\xi_{x_1}, \xi_{x_2}, \zeta_{x_1}$ and ζ_{x_2} will be calculated as

$$\begin{aligned} &\xi_{x_1} = \xi_{x_2} = 0, \\ &\zeta_{x_1} = -\frac{4}{3h^2}\left(\theta_{x_1} + \frac{\partial w}{\partial x_1} - \frac{v_0}{R_{x_1x_2}}\right), \\ &\zeta_{x_2} = -\frac{4}{3h^2}\left(\theta_{x_1} + \frac{\partial w}{\partial x_2} - \frac{u_0}{R_{x_1x_2}}\right) \end{aligned} \tag{12}$$

Replacing the unknown in Eq. (11), we obtain

$$\begin{aligned} &u(x_1,x_2,x_3) = \left(1+\frac{x_3}{R_{x_1}}\right)u_0 + \theta_{x_1}\left(x_3 - \frac{4x_3^3}{3h^2}\right) \\ &-\frac{\partial w_0}{\partial x_1}\left(\frac{4x_3^3}{3h^2}\right) + v_0\left(\frac{4x_3^3}{3h^2R_{x_1x_2}}\right) \\ &v(x_1,x_2,x_3) = \left(1+\frac{x_3}{R_{x_2}}\right)v_0 + \theta_{x_2}\left(x_3 - \frac{4x_3^3}{3h^2}\right) \\ &-\frac{\partial w_0}{\partial x_2}\left(\frac{4x_3^3}{3h^2}\right) + u_0\left(\frac{4x_3^3}{3h^2R_{x_1x_2}}\right) \\ &w(x_1,x_2,x_3) = w_0 \end{aligned} \tag{13}$$

For omitting C^1 continuity problem associated with TSDT, the out of plane derivatives are replaced by the following relations

$$\psi_{x_1} = \frac{\partial w_0}{\partial x_1},\ \psi_{x_2} = \frac{\partial w_0}{\partial x_2} \tag{14}$$

The final form of displacement filed expression owning C^0 continuity is written as

$$\begin{aligned} &u(x_1,x_2,x_3) = \left(1+\frac{x_3}{R_{x_1}}\right)u_0 + \theta_{x_1}\left(x_3 - \frac{4x_3^3}{3h^2}\right) \\ &-\psi_{x_1}\left(\frac{4x_3^3}{3h^2}\right) + v_0\left(\frac{4x_3^3}{3h^2R_{x_1x_2}}\right) \\ &v(x_1,x_2,x_3) = \left(1+\frac{x_3}{R_{x_2}}\right)v_0 + \theta_{x_2}\left(x_3 - \frac{4x_3^3}{3h^2}\right) \\ &-\psi_{x_2}\left(\frac{4x_3^3}{3h^2}\right) + u_0\left(\frac{4x_3^3}{3h^2R_{x_1x_2}}\right) \\ &w(x_1,x_2,x_3) = w_0 \end{aligned} \tag{15}$$

Hence, the field variables per node taken in the present investigation are u_0, v_0, w_0, θ_{x_1}, θ_{x_2}, Ψ_{x_1} and Ψ_{x_2}. Mathematically, it may be expressed as

$$\{\delta\} = \left\{u_0, v_0, w_0, \theta_{x_1}, \theta_{x_2}, \psi_{x_1}, \psi_{x_2}\right\}^T \tag{16}$$

where $\{\delta\}$ is termed as displacement vector.

The strain can be written as

$$\{\varepsilon\} = \left\{\varepsilon_{x_1}, \varepsilon_{x_2}, \gamma_{x_1x_2}, \gamma_{x_1x_3}, \gamma_{x_2x_3}\right\}^T \tag{17}$$

Further, the strain vector $\{\varepsilon\}$ can be correlated with global displacement vector $\{X\}$ by means of the following relationship.

$$\{\varepsilon\} = [B]\{X\} \tag{18}$$

Here $[B]$ is termed as strain-displacement matrix which contains the derivatives of shape functions.

The in-plane and transverse shear strains are

$$\begin{aligned} &\varepsilon_{x_1} = \frac{\partial u}{\partial x_1} + \frac{w}{R_{x_1}} \\ &\varepsilon_{x_2} = \frac{\partial v}{\partial x_2} + \frac{w}{R_{x_2}} \\ &\gamma_{x_1x_2} = \frac{\partial v}{\partial x_1} + \frac{\partial u}{\partial x_2} + \frac{2w}{R_{x_1x_2}} \\ &\gamma_{x_1x_3} = \frac{\partial u}{\partial x_3} + \frac{\partial w}{\partial x_1} - \frac{u_0}{R_{x_1}} - \frac{v_0}{R_{x_1x_2}} \\ &\gamma_{x_2x_3} = \frac{\partial v}{\partial x_3} + \frac{\partial w}{\partial x_2} - \frac{v_0}{R_{x_2}} - \frac{u_0}{R_{x_1x_2}} \end{aligned} \tag{19}$$

The strain relationship can be written as:

$$\begin{Bmatrix} \varepsilon_{x_1} \\ \varepsilon_{x_2} \\ \gamma_{x_1x_2} \end{Bmatrix} = \begin{Bmatrix} \varepsilon^0_{x_1} \\ \varepsilon^0_{x_2} \\ \gamma^0_{x_1x_2} \end{Bmatrix} + x_3\begin{Bmatrix} k_1^1 \\ k_2^1 \\ k_3^1 \end{Bmatrix} - \frac{4x_3^3}{3h^2}\begin{Bmatrix} k_1^3 \\ k_2^3 \\ k_2^3 \end{Bmatrix} \tag{20}$$

$$\begin{Bmatrix} \gamma_{x_1x_3} \\ \gamma_{x_2x_3} \end{Bmatrix} = \begin{Bmatrix} \gamma^0_{x_1x_3} \\ \gamma^0_{x_2x_3} \end{Bmatrix} - \frac{4x_3^2}{h^2}\begin{Bmatrix} k_4^2 \\ k_5^2 \end{Bmatrix} \tag{21}$$

where

$$\begin{aligned} &\varepsilon^0_{x_1} = \frac{\partial u_0}{\partial x_1} + \frac{w_0}{R_{x_1}}, \varepsilon^0_{x_2} = \frac{\partial v_0}{\partial x_2} + \frac{w_0}{R_{x_2}}, \\ &\gamma^0_{x_1x_2} = \frac{\partial v_0}{\partial x_1} + \frac{\partial u_0}{\partial x_2} + \frac{2w_0}{R_{x_1x_2}} \end{aligned} \tag{22}$$

$$\begin{aligned} &\gamma^0_{x_1x_3} = \left(\frac{\partial w_0}{\partial x_1} + \theta_{x_1}\right) - \frac{v_0}{R_{x_1x_2}}, \\ &\gamma^0_{x_2x_3} = \left(\frac{\partial w_0}{\partial x_2} + \theta_{x_2}\right) - \frac{u_0}{R_{x_1x_2}} \end{aligned} \tag{23}$$

$$k_1^1 = \frac{\partial \theta_{x_1}}{\partial x_1} + \frac{\partial u_0}{\partial x_1}\frac{1}{R_{x_1}}, k_2^1 = \frac{\partial \theta_{x_2}}{\partial x_2} + \frac{\partial v_0}{\partial x_2}\frac{1}{R_{x_2}},$$
$$k_3^1 = \left(\frac{\partial \theta_{x_2}}{\partial x_1} + \frac{\partial \theta_{x_1}}{\partial x_2}\right) + \left(\frac{\partial u_0}{\partial x_2}\frac{1}{R_{x_1}} + \frac{\partial v_0}{\partial x_1}\frac{1}{R_{x_2}}\right) \tag{24}$$

$$k_1^3 = \left(\frac{\partial \theta_{x_1}}{\partial x_1} + \frac{\partial \psi_{x_1}}{\partial x_1}\right) - \frac{\partial v_0}{\partial x_1}\frac{1}{R_{x_1x_2}},$$
$$k_2^3 = \left(\frac{\partial \theta_{x_2}}{\partial x_2} + \frac{\partial \psi_{x_2}}{\partial x_2}\right) - \frac{\partial u_0}{\partial x_2}\frac{1}{R_{x_1x_2}} \tag{25}$$

$$k_3^3 = \left(\frac{\partial \theta_{x_2}}{\partial x_1} + \frac{\partial \psi_{x_2}}{\partial x_1}\right) + \left(\frac{\partial \theta_{x_1}}{\partial x_2} + \frac{\partial \psi_{x_1}}{\partial x_2}\right)$$
$$+ \left(\frac{\partial u_0}{\partial x_1} + \frac{\partial v_0}{\partial x_2}\right)\frac{1}{R_{x_1x_2}} \tag{26}$$

$$k_4^2 = \left(\theta_{x_1} + \psi_{x_1}\right) - \frac{v_0}{R_{x_1x_2}}, k_5^2 = \left(\theta_{x_2} + \psi_{x_2}\right) - \frac{u_0}{R_{x_1x_2}} \tag{27}$$

3.2 Constitutive relationship

The linear stress-strain constitutive relationship for the FGM conoidal shell are

$$\{\sigma\} = [Q]\{\varepsilon\} \tag{28}$$

where the constitutive matrix

$$[Q] = \begin{bmatrix} Q_{11} & Q_{12} & 0 & 0 & 0 \\ Q_{21} & Q_{22} & 0 & 0 & 0 \\ 0 & 0 & Q_{33} & 0 & 0 \\ 0 & 0 & 0 & Q_{44} & 0 \\ 0 & 0 & 0 & 0 & Q_{55} \end{bmatrix} \tag{29}$$

where the term Q_{ij} can be obtained with the help of the Poisson's ratio (ν) and Young's modulus (E) which is a function of thickness coordinate.

$$Q_{11} = Q_{22} = \frac{E(x_3)}{1-\nu^2},\ Q_{12} = Q_{21} = \frac{\nu E(x_3)}{1-\nu^2},$$
$$Q_{33} = Q_{44} = Q_{55} = \frac{E(x_3)}{2(1+\nu)} \tag{30}$$

4. Finite element modelling

4.1 Introduction

For the present C^0 finite element (FE) model, nine noded isoparametric Lagrangian element with seven degrees of freedom at each node is utilized in the present investigation. The shape function (interpolation function) is used to express the generalized displacement vector and element geometry at any point within an element as

$$\{\delta\} = \sum_{i=1}^{9} N_i(\xi,\eta)\{\delta\}_i \tag{31}$$

$$\{x_1\} = \sum_{i=1}^{9} N_i(\xi,\eta)\{x_1\}_i \tag{32}$$

$$\{x_2\} = \sum_{i=1}^{9} N_i(\xi,\eta)\{x_2\}_i \tag{33}$$

The shape functions N_i of nine noded isoprametric Lagrangian element are described below.

For corner nodes:

$$N_1 = \frac{1}{4}(\xi-1)(\eta-1)\xi\eta,\ N_3 = \frac{1}{4}(\xi+1)(\eta-1)\xi\eta$$

$$N_7 = \frac{1}{4}(\xi-1)(\eta+1)\xi\eta,\ N_9 = \frac{1}{4}(\xi+1)(\eta+1)\xi\eta$$

For mid nodes:

$$N_2 = \frac{1}{2}\left(1-\xi^2\right)\left(\eta^2-\eta\right),\ N_4 = \frac{1}{2}\left(\xi^2-\xi\right)\left(1-\eta^2\right)$$

$$N_6 = \frac{1}{2}\left(\xi^2+\xi\right)\left(1-\eta^2\right),\ N_8 = \frac{1}{2}\left(1-\xi^2\right)\left(\eta^2+\eta\right)$$

For centre node:

$$N_5 = \left(1-\xi^2\right)\left(1-\eta^2\right)$$

4.2 Skew boundary transformation of shell

For rhombic shell (the plan is shown in Fig. 3), it is necessary to transform the element matrices from global to local axes because the edges of boundary elements are not parallel to the global axes of the conoidal shell. Therefore, a transformation matrix [T] is required to transform the element matrices from global to local axes.

Transformation matrix

$$[T] = \begin{pmatrix} c & -s & 0 & 0 & 0 & 0 & 0 \\ s & c & 0 & 0 & 0 & 0 & 0 \\ 0 & 0 & 1 & 0 & 0 & 0 & 0 \\ 0 & 0 & 0 & c & -s & 0 & 0 \\ 0 & 0 & 0 & s & c & 0 & 0 \\ 0 & 0 & 0 & 0 & 0 & c & -s \\ 0 & 0 & 0 & 0 & 0 & s & c \end{pmatrix} \tag{34}$$

where c = cosα, s = sinα and α is known as skew angle.

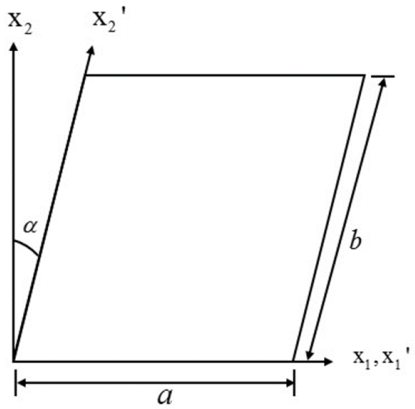

Fig. 3 Plan view of rhombic shell

4.3 Governing equation

The strain energy may be expressed as

$$U = \frac{1}{2}\iiint \{\varepsilon\}^T \{\sigma\} \mathrm{d}x_1 \mathrm{d}x_2 \mathrm{d}x_3 \tag{35}$$

By using the Eq. (28), the above expression can be represented as

$$U = \frac{1}{2}\iint \{\varepsilon\}^T [D] \{\varepsilon\} \mathrm{d}x_1 \mathrm{d}x_2 \tag{36}$$

where, $[D] = \int [H]^T [Q][H] dx_3$ in which $[H]$ is the matrix that contains the terms involving x_3 and h.

By utilizing Eq. (18) the stiffness matrix $[K]$ is written as

$$[K] = \iint [B]^T [D][B] \mathrm{d}x_1 \mathrm{d}x_2 \tag{37}$$

5. Results and discussion

In this section, the bending analysis of FGM sandwich rhombic conoidal shells are analysed under various type of mechanical loading. Parameters like thickness ratio, aspect ratio, *hl/hh* ratio, volume fraction index, skew angle and boundary conditions are also accomplished for numerical results. Unless otherwise stated, the following non-dimensional quantities are considered in the forthcoming examples.

The loading pattern used in the present analysis are written below:

$$q = q_0,\ q = q_0 \sin\left(\frac{\pi x_1}{a}\right)\sin\left(\frac{\pi x_2}{b}\right),$$

$$q = q_0 \cos\left(\frac{\pi x_1}{a}\right)\sin\left(\frac{\pi x_2}{b}\right)$$

$$q = q_0 \cos\left(\frac{\pi x_1}{a}\right)\cos\left(\frac{\pi x_2}{b}\right)$$

Non-dimensional quantities used for FGM rhombic conoidal shell and FGM sandwich conoidal shell with homogenous core are:

$$\bar{w} = w\frac{10hE_0}{q_0 a^2},\ \bar{\sigma}_{x_1} = \sigma_{x_1}\left(\frac{a}{2},\frac{b}{2},\frac{h}{2}\right)\frac{10h^2}{q_0 a^2},$$

$$\bar{\sigma}_{x_2} = \sigma_{x_2}\left(\frac{a}{2},\frac{b}{2},\frac{h}{2}\right)\frac{10h^2}{q_0 a^2},$$

$$\bar{\tau}_{x_1x_2} = \tau_{x_1x_2}\left(0,0,-\frac{h}{2}\right)\frac{h}{q_0 a}$$

Non-dimensional quantities used for FGM sandwich conoidal shell with isotropic skins are:

$$\bar{w} = w\frac{10h^3E_c}{q_0 a^4},\bar{\sigma}_{x_1} = \sigma_{x_1}\left(\frac{a}{2},\frac{b}{2},\frac{h}{2}\right)\frac{h}{q_0 a},$$

$$\bar{\sigma}_{x_2} = \sigma_{x_2}\left(\frac{a}{2},\frac{b}{2},\frac{h}{2}\right)\frac{h}{q_0 a},$$

$$\bar{\tau}_{x_1x_2} = \tau_{x_1x_2}\left(0,0,-\frac{h}{2}\right)\frac{h}{q_0 a}$$

The details of some of the boundary conditions used the present analysis:

1. Clamped (CCCC):

$$u = v = w = \theta_{x_1} = \theta_{x_2} = \psi_{x_1} = \psi_{x_2} = 0,$$

at $x_1 = 0, a$ and $x_2 = 0, b$

2. Simply supported (SSSS):

$$v = w = \theta_{x_2} = \Psi_{x_2} = 0, \text{ at } x_1 = 0, a$$

$$u = w = \theta_{x_1} = \Psi_{x_1} = 0, \text{ at } x_2 = 0, b$$

3. Clamped and simply supported (CCSS):

$$u = v = w = \theta_{x_1} = \theta_{x_2} = \Psi_{x_1} = \Psi_{x_2} = 0, \text{ at } x_1 = 0, a$$

$$u = w = \theta_{x_1} = \Psi_{x_1} = 0, \text{ at } x_2 = 0, b$$

5.1 Convergence and validation study

In order to check the consistency and the stability of present FE results, three appropriate examples have been solved. No results are available for FGM sandwich conoidal shell in literature, hence the consistency of the present model has been checked by comparing dimensionless deflection for FGM sandwich plate and isotropic conoidal shell with available results in the literature. The following material properties of the FGM components used in present study are:

FGM- 1 (Al/ZrO_2): E_c = 151 GPa, E_m = 70 GPa, $\nu_c = \nu_m$ = 0.3, ρ_c = 3000 kg/m^3, ρ_m = 2707 kg/m^3

FGM- 2 (Al/Al_2O_3): E_c = 380 GPa, E_m = 70 GPa, $\nu_c = \nu_m$ = 0.3, ρ_c = 3800 kg/m^3, ρ_m = 3000 kg/m^3

Table 1 The convergence study for non-dimensional maximum deflection of simply supported FGM-1 plate

Mesh	Volume fraction index			
	Ceramic	0.5	1	Metal
6x6	0.02480	0.03329	0.03680	0.05350
8x8	0.02481	0.03331	0.03685	0.05352
12x12	0.02482	0.03333	0.03688	0.05353
16x16	0.02482	0.03333	0.03688	0.05353
Ferreira *et al*. (2007)	0.0248	0.0330	0.0368	0.0536

Table 2 Comparison of the dimensionless transverse central displacements of the FGM sandwich plate

n	Thickness scheme	Abdelaziz *et al*. (2011) RPT	Zenkour (2013) FSDPT	Zenkour (2013) TSDPT	Zenkour (2013) SSDPT	Present
0	1-0-1	0.19606	0.19607	0.19606	0.19605	0.19606
	1-1-1	0.19606	0.19607	0.19606	0.19605	0.19606
	1-2-1	0.19606	0.19607	0.19606	0.19605	0.19606
	2-1-2	0.19606	0.19607	0.19606	0.19605	0.19606
	2-2-1	0.19606	0.19607	0.19606	0.19605	0.19606
1	1-0-1	0.32358	0.32484	0.32358	0.32349	0.33354
	1-1-1	0.29199	0.29301	0.29199	0.29194	0.29686
	1-2-1	0.27094	0.27167	0.27094	0.27093	0.27353
	2-1-2	0.30631	0.30750	0.30632	0.30624	0.31316
	2-2-1	0.28025	0.28168	0.28085	0.28082	0.28391
5	1-0-1	0.40927	0.41120	0.40927	0.40905	0.40580
	1-1-1	0.37144	0.37356	0.37145	0.37128	0.36403
	1-2-1	0.33480	0.33631	0.33480	0.33474	0.32704
	2-1-2	0.39182	0.39418	0.39183	0.39160	0.38582
	2-2-1	0.34960	0.35123	0.34960	0.34950	0.34032
10	1-0-1	0.41772	0.41919	0.41772	0.41750	0.41464
	1-1-1	0.38551	0.38787	0.38551	0.38490	0.37778
	1-2-1	0.34823	0.34996	0.34824	0.34119	0.33953
	2-1-2	0.40407	0.40657	0.40407	0.40376	0.3984
	2-2-1	0.36212	0.36395	0.34916	0.35577	0.35202

RPT: refined plate theory; FSDPT: first order shear deformation plate theory; TSDPT: third order shear deformation plate theory; SSDPT: sinusoidal shear deformation plate theory

Example 1. In the present example, the convergence behaviour of the dimensionless maximum deflection of FGM-1 (Al/ZrO2) plate is examined for four power law indices (n = 0, 0.5, 1, ∞) and presented in Table 1. For this particular example, we used hl = 0 and hh = 0 in the present FE code of the FGM conoidal shell for converting it into FGM plate. Based on convergence study, it is found that at 16 × 16 mesh size, the results are converging for the present nine noded isoparametric elements. From Table 1, it is noted that our numerical results are consistent with Ferreira *et al*. (2007).

Example 2. Tables 2-3 represents the comparison of dimensionless transverse displacement and dimensionless axial stress of simply supported FGM sandwich plate. The results are calculated for FGM sandwich plate having an isotropic core. The value of the thickness ratio (a/h) is taken as 10. Different values of volume fraction index (n = 0, 1, 2, 5 and 10) are taken for the comparison. The non-dimensional deflection for various type of thickness scheme is compared with available results of different theories. This concurs well with the available results in the literature.

Example 3. No results available in literature for FGM conoidal shell, hence present FE result of FGM conoidal shell are validated with isotropic conoidal shell results. The Poisson's ratio v = 0.15, hl/hh = 0.5, side-to-thickness ratio a/h = 19 and simply supported boundary condition is used to validate present result. Table 4 shows the validation of present FE formulation with Hadid (1964) and Bakshi and Chakravorty (2014).

The validation study confirms the betterment of present FE result over Bakshi and Chakravorty (2014) as the present results are more close to elasticity results given by Hadid (1964).

Table 3 Comparison of the dimensionless axial stress ($a/2$, $b/2$, $h/2$) of the FGM square sandwich plate

n	Thickness scheme	Zenkour (2013) FSDPT	Zenkour (2013) TSDPT	Zenkour (2013) SSDPT	Present
0	1-0-1	1.97576	2.04985	2.05452	1.99789
	1-1-1	1.97576	2.04985	2.05452	1.99789
	1-2-1	1.97576	2.04985	2.05452	1.99789
	2-1-2	1.97576	2.04985	2.05452	1.99789
	2-2-1	1.97576	2.04985	2.05452	1.99789
1	1-0-1	1.53245	1.57923	1.58204	1.59447
	1-1-1	1.38303	1.42617	1.42892	1.41904
	1-2-1	1.28096	1.32309	1.32590	1.30662
	2-1-2	1.45167	1.49587	1.49859	1.49777
	2-2-1	1.27749	1.32062	1.32342	1.38722
2	1-0-1	1.77085	1.82167	1.82450	1.79421
	1-1-1	1.58242	1.62748	1.63025	1.58602
	1-2-1	1.43580	1.47988	1.48283	1.43611
	2-1-2	1.67496	1.72144	1.72412	1.68520
	2-2-1	1.42528	1.47095	1.47387	1.54003
10	1-0-1	1.96780	2.03036	2.03360	1.97430
	1-1-1	1.83754	1.88376	1.88147	1.80937
	1-2-1	1.65844	1.70417	1.64851	1.62762
	2-1-2	1.92165	1.97126	1.97313	1.90572
	2-2-1	1.61645	1.66660	1.61979	1.75485

FSDPT: first order shear deformation plate theory; TSDPT: third order shear deformation plate theory; SSDPT: sinusoidal shear deformation plate theory

Table 4 Comparison of deflection ($x10^{-2}$) of isotropic conoid under uniformly distributed load along $x_2/b = 0.50$

x_1/a	Bakshi and Chakravorty (2014)	Hadid (1964)	Present
0.10	2.3680	2.5231	2.5621
0.40	5.1557	4.6333	4.7609
0.60	4.0510	3.5448	3.8575
0.70	3.4129	3.3149	3.2970
0.80	2.4809	2.5544	2.5949

Table 5 Comparison of non-dimensional stress at the centroid of the top and bottom surface of simply supported FGM-2 plate

Skew angle	Maximum deflection		Stress at top	
	Kulkarni *et al.* (2015)	Present	Kulkarni *et al.* (2015)	Present
15	4.1890	4.1881	0.2694	0.2695
30	2.9687	2.9658	0.2147	0.2147
45	1.5337	1.5327	0.1397	0.1386

Example 4. In this example, comparison of non-dimensional deflection and stress of simply supported FGM-2 rhombic plate is presented in Table 5. The skew plate is ceramic. For different skew angle the maximum deflection and normal stress of skew plate were compared and it shows present results are again in good agreement with the published results with Kulkarni *et al*. (2015).

5.2 Results and discussion

To analyze FGM conoidal shells under various type of transverse loading, different composition of material constituents, different combination of boundary condition, numerous value of volume fraction index, side-to-thickness ratio, aspect ratio and *hl/hh* ratio are considered.

Table 6 represent the dimensionless maximum deflection and their location of FGM-1 rhombic conoidal shell subjected to uniform loading. The results were computed for $a/b = 1$ and $hl/hh = 0.25$ ($hl = 0.05$ and $hh = 0.2$). These numerical values revealed that as we move from $n = 0$ to $n = 10$, the deflection of the conoidal shell is increased and it may be attributed to the higher value of volume fraction index of the shell which lead to lesser ceramic content and thus reducing its stiffness. It is anticipated that there is nearly 32% increase in the maximum deflection of the FGM-1 rhombic shell for all skew angle as the volume fraction index changed from $n = 0$ to $n = 1$. The maximum dimensionless deflection increased along with the thickness of rhombic shell while with an increase in skew angle, a decrease in dimensionless deflection is noticed. Due to the fact that the length of shorter diagonal is reduced when skew angle increases and shortening of diagonal leads to enhancement in stiffness of the rhombic shell thus the deflection reduces. Numerical results of non-dimensional stresses of FGM-1 rhombic conoidal shell subjected to uniform loading is presented in Table 7.

Table 6 Non-dimensional maximum deflection of simply supported FGM-1 rhombic conoidal shell under uniform loading

a/h	*α*	Non-dimensional maximum deflection				
		Ceramic	0.2	0.5	1	10
10	15°	0.09141 (0.52,0.46)	0.10268 (0.52,0.46)	0.11116 (0.52,0.46)	0.12224 (0.52,0.46)	0.15470 (0.49,0.46)
	30°	0.05090 (0.60,0.39)	0.05717 (0.60,0.39)	0.06196 (0.60,0.39	0.06823 (0.60,0.39)	0.09666 (0.60,0.39
	45°	0.02014 (0.63,0.28)	0.02263 (0.63,0.28)	0.02458 (0.63,0.28)	0.02615 (0.63,0.28)	0.04019 (0.63,0.28)
	60°	0.00547 (0.63,0.175)	0.00615 (0.63,0.175)	0.00653 (0.63,0.175)	0.00716 (0.63,0.175	0.01047 (0.63,0.175)
20	15°	0.03146 (0.41,0.41)	0.03506 (0.42,0.44)	0.04030 (0.42,0.44)	0.0424 (0.42,0.44)	0.05900 (0.41,0.41)
	30°	0.01676 (0.48,0.32)	0.02025 (0.487,0.32)	0.02105 (0.487,0.32)	0.02335 (0.487,0.32)	0.03328 (0.46,0.32)
	45°	0.00801 (0.50,0.23)	0.00874 (0.50,0.23)	0.00946 (0.52,0.25)	0.01061 (0.52,0.25)	0.00150 (0.50,0.23)
	60°	0.00179 (0.51,0.137)	0.00224 (0.53,0.15)	0.00217 (0.53,0.15)	0.00240 (0.53,0.15)	0.00370 (0.51,0.137)

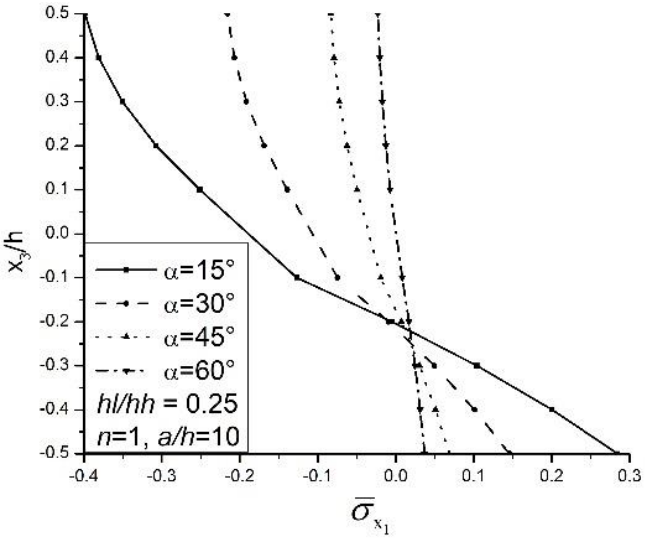

Fig. 4 Effect of skew angle on dimensionless axial stress of FGM-1 rhombic conoidal shell under uniform loading

The dimensionless value of normal stress decreases with increase in skew angle of the conoidal shell. Value of $\bar{\sigma}_{x_1}$ approximately decreases by 95% when the skew angle changed from 15° to 45° for FGM rhombic conoidal shell. It can be seen from Fig. 4; the maximum dimensionless stress occurs at top of the rhombic conoidal shell. Sharply reduction in stress is noticed for smaller skew angle, as skew angle increases, very small reduction in stresses in the thickness direction was noticed.

The non-dimensional deflection of the FGM-1 Type-I sandwich rhombic conoidal shell is presented in Table 8. Five cases of thickness scheme and volume fraction index (n = 0, 0.2, 0.5, 1 and 10) are used. The aspect ratio a/b = 1 and minimum rise to maximum rise ratio hl/hh = 0.25 are selected. Similar to the rhombic conoidal shell, the dimensionless deflection of sandwich rhombic conoidal shell decreases with increase in skew angle and increases with increases in volume fraction index for all type of thickness scheme.

It can be observed from Fig. 5 that the maximum deflection of the sandwich conoidal shell occurs at a different location, unlike plate structure where maximum deflection occurs at the midpoint. The negative value of deflection is noticed for skew angle more than 30° under sin-sin loading.

The dimensionless stresses of FGM-1 Type-I sandwich rhombic conoidal shell for various value of thickness scheme are presented in Table 9. Fig. 6 shows the variation of normal stresses in thickness coordinate for various value of skew angles. It can be seen that when skew angle increases the stress variation along the thickness is reduced due to higher stiffness provided by skew angle. Effect of boundary condition on Type-I (1-2-1) sandwich rhombic conoidal shell made of FGM-1 is presented in Table 10.

CCCC has the lowest deflection due to the stiffness of the boundary condition while CFCF has the highest dimensionless deflection. For all type of boundary support, the deflection decreases with increase in skew angle. The correlation between hl/hh ratio and dimensionless deflection of FGM-1 Type-I sandwich rhombic conoidal shell was tested in Table 11. Interestingly, for higher value of hl/hh ratio, lower value of dimensionless deflection is noticed irrespective of skew angle and loading pattern. The decrease in hl/hh ratio reduces the curvature of the lower end (hl) of the conoidal shell, due to this the stiffness of shell reduces, thus deflection increases. Also, maximum deflection is spotted in uniform loading while minimum deflection occurs when the Type-1 sandwich conoidal shell is subjected to cos-cos loading same as the rhombic conoidal shell.

The variation of dimensionless deflection of Type-II (1-8-1) sandwich rhombic conoidal shell made of FGM-2 is shown in Fig. 7 subjected to sin-sin loading, respectively. hl = 0.05, hh = 0.2 (hl/hh = 0.25) and a/h = 10 was used. A negative value of defection is noticed for skew angle more than 30° and more, due to nature of sin-sin loading. It can be noted here the dimensionless deflection is decreased when skew angle increases, due to the fact that skewness of shell offers high stiffness.

Table 7 Non-dimensional stress variation of simply supported FGM-1 rhombic conoidal shell under uniform loading

n	α	$a/h = 10$			$a/h = 20$		
		$\bar{\sigma}_{x_1}$	$\bar{\sigma}_{x_2}$	$\bar{\tau}_{x_1x_2}$	$\bar{\sigma}_{x_1}$	$\bar{\sigma}_{x_2}$	$\bar{\tau}_{x_1x_2}$
Ceramic	15°	-0.62727	-1.0353	-0.18408	-0.3397	-0.9169	-0.2299
	30°	-0.34064	-0.7515	-0.01314	-0.1409	-0.65016	-0.0121
	45°	-0.12794	-0.4576	0.00825	-0.0326	-0.38461	0.0227
	60°	-0.03091	-0.2094	0.01289	-0.0016	-0.16578	0.0231
0.2	15°	-0.33042	-0.5707	-0.20008	-0.1780	-0.52779	-0.2601
	30°	-0.17806	-0.4143	-0.01635	-0.0767	-0.37899	-0.0270
	45°	-0.06760	-0.2532	0.00803	-0.0217	-0.22749	0.0181
	60°	-0.01786	-0.1181	0.01343	-0.0042	-0.10073	0.0236
0.5	15°	-0.36062	-0.6293	-0.20076	-0.1958	-0.59045	-0.2625
	30°	-0.19483	-0.4573	-0.06909	-0.0859	-0.42532	-0.0275
	45°	-0.07471	-0.2800	0.00986	-0.0259	-0.25629	0.0203
	60°	-0.02029	-0.1312	0.01520	-0.0059	-0.11436	0.0263
1	15°	-0.39854	-0.7003	-0.19513	-0.2173	-0.66301	-0.2562
	30°	-0.21570	-0.5092	-0.01320	-0.0966	-0.47854	-0.0249
	45°	-0.08330	-0.3122	0.01226	-0.0303	-0.28905	0.0235
	60°	-0.02303	-0.1467	0.01698	-0.0075	-0.1296	0.0289
10	15°	-0.53702	-0.9140	-0.16253	-0.2785	-0.81602	-0.2057
	30°	-0.28613	-0.6595	-0.00836	-0.1151	-0.5819	-0.0073
	45°	-0.10568	-0.3999	0.01058	-0.0283	-0.34607	0.0253
	60°	-0.02620	-0.1832	0.01335	-0.0028	-0.14999	0.0240

Table 8 Maximum non-dimensional deflection of FGM-1 Type-I sandwich rhombic conoidal shell under sin-sin load

n	α	Non-dimensional maximum deflection				
		1-0-1	1-1-1	1-2-1	2-1-2	2-2-1
0	15°	0.04488 (0.50,0.46)	0.04488 (0.50,0.46)	0.04488 (0.50,0.46)	0.04488 (0.50,0.46)	0.04488 (0.50,0.46)
	30°	0.02640 (0.55,0.39)	0.02640 (0.55,0.39)	0.02640 (0.55,0.39)	0.02640 (0.55,0.39)	0.02640 (0.55,0.39)
	45°	0.01182 (0.58,0.28)	0.01182 (0.58,0.28)	0.01182 (0.58,0.28)	0.01182 (0.58,0.28)	0.01182 (0.58,0.28)
	60°	0.00327 (0.62,0.19)	0.00327 (0.62,0.19)	0.00327 (0.62,0.19)	0.00327 (0.62,0.19)	0.00327 (0.62,0.19)
0.2	15°	0.05371 (0.50,0.46)	0.05086 (0.50,0.46)	0.04941 (0.50,0.46)	0.05201 (0.50,0.46)	0.05067 (0.50,0.46)
	30°	0.03170 (0.55,0.39)	0.03000 (0.55,0.39)	0.02913 (0.55,0.39)	0.03069 (0.55,0.39)	0.02987 (0.55,0.39)
	45°	0.01417 (0.58,0.28)	0.01342 (0.58,0.28)	0.01303 (0.58,0.28)	0.01372 (0.58,0.28)	0.01338 (0.58,0.28)
	60°	0.00386 (0.62,0.19)	0.00367 (0.62,0.20)	0.00357 (0.62,0.20)	0.00375 (0.62,0.20)	0.00367 (0.62,0.19)
0.5	15°	0.05943 (0.50,0.46)	0.05468 (0.50,0.46)	0.05227 (0.50,0.46)	0.05659 (0.50,0.46)	0.05432 (0.50,0.46)
	30°	0.03511 (0.55,0.39)	0.03230 (0.55,0.39)	0.03085 (0.55,0.39)	0.03343 (0.55,0.39)	0.03205 (0.55,0.39)
	45°	0.01569 (0.58,0.28)	0.01444 (0.58,0.28)	0.01380 (0.58,0.28)	0.01494 (0.58,0.28)	0.01437 (0.58,0.28)
	60°	0.00425 (0.62,0.19)	0.00392 (0.62,0.20)	0.00376 (0.62,0.20)	0.00405 (0.60,0.19)	0.00392 (0.60,0.19)
1	15°	0.06637 (0.50,0.46)	0.05913 (0.50,0.46)	0.05553 (0.50,0.46)	0.06202 (0.50,0.46)	0.05855 (0.50,0.46)
	30°	0.03925 (0.55,0.39)	0.03498 (0.55,0.39)	0.03282 (0.55,0.39)	0.03669 (0.55,0.39)	0.03458 (0.55,0.39)
	45°	0.01753 (0.58,0.28)	0.01563 (0.58,0.28)	0.01467 (0.58,0.28)	0.01639 (0.58,0.28)	0.01551 (0.58,0.28)
	60°	0.00473 (0.62,0.19)	0.00422 (0.60,0.19)	0.00398 (0.62,0.20)	0.00442 (0.60,0.19)	0.00422 (0.60,0.19)
10	15°	0.08682 (0.50,0.46)	0.07163 (0.50,0.46)	0.06453 (0.50,0.46)	0.07745 (0.50,0.46)	0.07017 (0.50,0.46)
	30°	0.05121 (0.55,0.39)	0.04245 (0.55,0.39)	0.03825 (0.55,0.39)	0.04584 (0.55,0.39)	0.04156 (0.54,0.37)
	45°	0.02287 (0.58,0.28)	0.01895 (0.58,0.28)	0.01708 (0.58,0.28)	0.02046 (0.58,0.28)	0.01866 (0.58,0.28)
	60°	0.00622 (0.62,0.19)	0.00508 (0.60,0.19)	0.00458 (0.60,0.19)	0.00550 (0.60,0.19)	0.00506 (0.60,0.19)

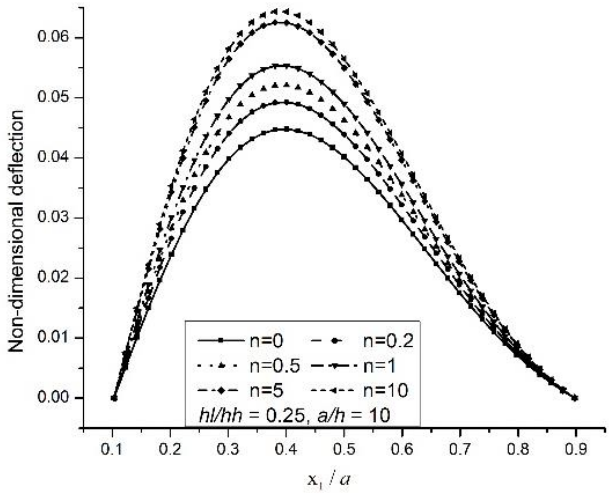

(a) 15°

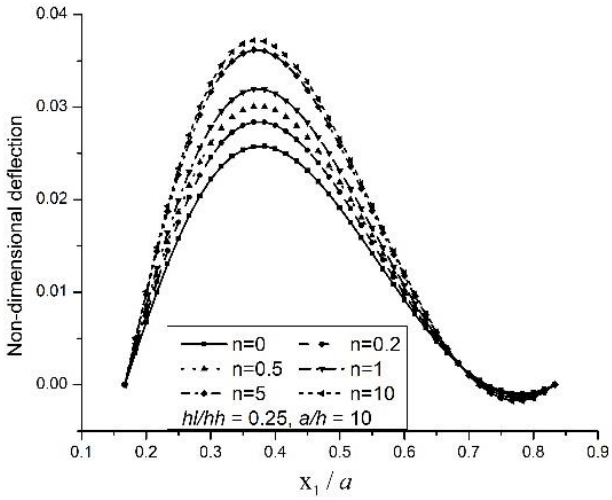

(b) 30°

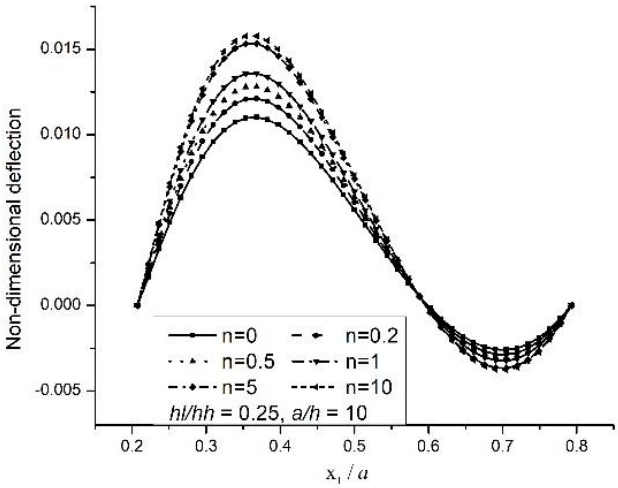

(c) 45°

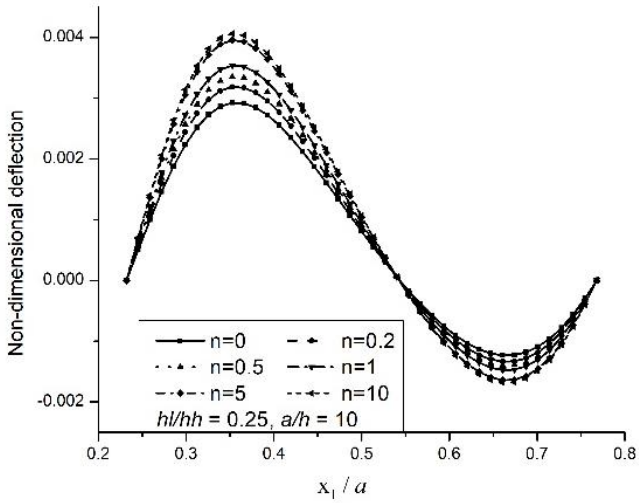

(d) 60°

Fig. 5 Variation of non-dimensional deflection along center line of FGM-1 Type-I (1-2-1) sandwich rhombic conoidal shell for four skew angles subjected to sin-sin loading

Table 9 Dimensionless normal stress of FGM-1 Type-I sandwich rhombic conoidal shell under sin-sin load (n = 1)

Stresses	α	Non-dimensional stress				
		1-0-1	1-1-1	1-2-1	2-1-2	2-2-1
$\bar{\sigma}_{x_1}$	15°	-0.3971	-0.3540	-0.3329	-0.3711	-0.3410
	30°	-0.2135	-0.1904	-0.1796	-0.1993	-0.1835
	45°	-0.0768	-0.0685	-0.0650	-0.0716	-0.0664
	60°	-0.0173	-0.0155	-0.0148	-0.0162	-0.0150
$\bar{\sigma}_{x_2}$	15°	-0.6268	-0.5587	-0.5235	-0.5862	-0.5321
	30°	-0.4041	-0.3604	-0.3381	-0.3780	-0.3429
	45°	-0.1924	-0.1718	-0.1615	-0.1800	-0.1634
	60°	-0.0620	-0.0555	-0.0524	-0.0580	-0.0527
$\bar{\tau}_{x_1x_2}$	15°	-0.3562	-0.0516	-0.0460	-0.0430	-0.0483
	30°	-0.1923	0.0025	0.0022	0.0020	0.0023
	45°	-0.0697	0.0113	0.0101	0.0095	0.0106
	60°	-0.0158	0.0129	0.0115	0.0109	0.0120

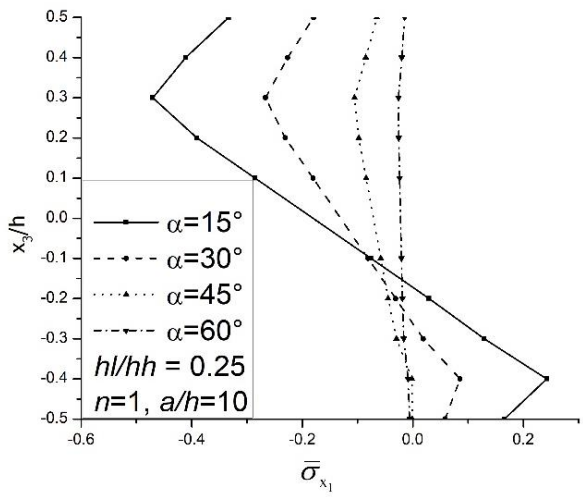

Fig. 6 Effect of skew angle on dimensionless axial stress of FGM-1 Type-I sandwich rhombic conoidal shell under sin-sin loading.

Table 10 Deflection of FGM-1 Type-I (1-2-1) sandwich rhombic conoidal shell for different type of boundary constraints

a/h	*α*	Non-dimensional maximum deflection				
		CCCC	CCSS	CSCS	CCFF	CFCF
10	15°	0.04275 (0.55,0.48)	0.04520 (0.55,0.46)	0.04422 (0.55,0.48)	0.08945 (0.56,0.41)	0.23283 (0.98,0.97)
	30°	0.02388 (0.61,0.41)	0.02530 (0.60,0.39)	0.02416 (0.61,0.41)	0.06049 (0.525,0.0)	0.02835 (0.61,0.41)
	45°	0.00965 (0.65,0.30)	0.01043 (0.63,0.28)	0.00981 (0.65,0.30)	0.03961 (0.55,0.0)	0.01186 (0.11,0.71)
	60°	0.00249 (0.67,0.20)	0.00268 (0.65,0.19)	0.00253 (0.67,0.20)	0.01677 (0.575,0.0)	0.10069 (0.19,0.50)
20	15°	0.07395 (0.50,0.46)	0.07440 (0.50,0.46)	0.07438 (0.50,0.48)	0.16743 (0.53,0.38)	0.55580 (0.10,0.96)
	30°	0.04072 (0.57,0.39)	0.04141 (0.575,0.39)	0.04140 (0.575,0.39)	0.13425 (0.475,0.0)	0.05045 (0.11,0.19)
	45°	0.01572 (0.62,0.30)	0.01611 (0.61,0.28)	0.01607 (0.62,0.30)	0.09330 (0.50,0.0)	0.08469 (0.11,0.14)
	60°	0.00364 (0.65,0.20)	0.00372 (0.62,0.19)	0.00369 (0.64,0.20)	0.04290 (0.55,0.0)	0.07944 (0.11,0.10)

Table 11 Deflection of FGM-1 Type-I (1-2-1) sandwich rhombic conoidal shell subjected to different type of loading

hl/hh	Load	Non-dimensional maximum deflection			
		15°	30°	45°	60°
0.25	uniform	0.07523 (0.50,0.46)	0.04243 (0.56.0.37)	0.01778 (0.61,0.28)	0.00452 (0.63,0.175)
	sin-sin	0.05553 (0.50,0.46)	0.03282 (0.55,0.39)	0.01467 (0.58,0.28)	0.00398 (0.62,0.20)
	cos-sin	0.01410 (0.29,0.34)	0.00600 (0.325,0.22)	0.00229 (0.36,0.16)	0.00062 (0.37,0.11)
	cos-cos	0.02010 (0.87,0.75)	0.01723 (0.94,0.67)	0.00943 (0.950.56)	0.00359 (1.0,0.39)
0.20	uniform	0.07895 (0.50,0.46)	0.04405 (0.56.0.37)	0.01836 (0.61,0.28)	0.00467 (0.63,0.175)
	sin-sin	0.05796 (0.50,0.46)	0.03388 (0.55,0.39)	0.01505 (0.58,0.28)	0.00408 (0.62,0.19)
	cos-sin	0.01423 (0.29,0.34)	0.00594 (0.325,0.22)	0.00226 (0.36,0.16)	0.00062 (0.37,0.11)
	cos-cos	0.02004 (0.87,0.75)	0.01716 (0.94,0.67)	0.00939 (0.950.56)	0.00358 (1.0,0.39)
0.15	uniform	0.08283 (0.50,0.46)	0.04572 (0.56.0.37)	0.01895 (0.61,0.28)	0.00483 (0.63,0.175)
	sin-sin	0.06050 (0.50,0.46)	0.03498 (0.55,0.39)	0.01544 (0.58,0.28)	0.00419 (0.62,0.19)
	cos-sin	0.01433 (0.29,0.34)	0.00586 (0.325,0.22)	0.00223 (0.36,0.16)	0.00062 (0.37,0.11)
	cos-cos	0.01999 (0.87,0.75)	0.01709 (0.94,0.67)	0.00936 (0.950.56)	0.00357 (1.0,0.39)
0.10	uniform	0.08686 (0.50,0.46)	0.04744 (0.56.0.37)	0.01956 (0.61,0.28)	0.00499 (0.60,0.175)
	sin-sin	0.06312 (0.50,0.46)	0.03610 (0.55,0.39)	0.01584 (0.58,0.28)	0.00429 (0.62,0.19)
	cos-sin	0.01440 (0.29,0.34)	0.00578 (0.325,0.22)	0.00220 (0.36,0.16)	0.00062 (0.37,0.11)
	cos-cos	0.01992 (0.87,0.75)	0.01701 (0.94,0.67)	0.00933 (0.950.56)	0.00356 (1.0,0.39)
0.05	uniform	0.09102 (0.50,0.46)	0.04921 (0.56.0.37)	0.02018 (0.61,0.28)	0.00516 (0.60,0.175)
	sin-sin	0.06584 (0.50,0.46)	0.03725 (0.55,0.39)	0.01624 (0.58,0.28)	0.00441 (0.62,0.19)
	cos-sin	0.01445 (0.29,0.34)	0.00568 (0.325,0.22)	0.00216 (0.36,0.16)	0.00062 (0.37,0.11)
	cos-cos	0.01986 (0.87,0.75)	0.01693 (0.94,0.67)	0.00929 (0.950.56)	0.00356 (1.0,0.39)
0.00	uniform	0.09531 (0.50,0.46)	0.05103 (0.56.0.37)	0.02082 (0.61,0.28)	0.00533 (0.60,0.175)
	sin-sin	0.06862 (0.50,0.46)	0.03843 (0.55,0.39)	0.01665 (0.58,0.28)	0.00452 (0.62,0.19)
	cos-sin	0.01446 (0.29,0.34)	0.00557 (0.325,0.22)	0.00213 (0.36,0.16)	0.00061 (0.37,0.11)
	cos-cos	0.01979 (0.87,0.75)	0.01685 (0.94,0.67)	0.00925 (0.950.56)	0.00355 (1.0,0.39)

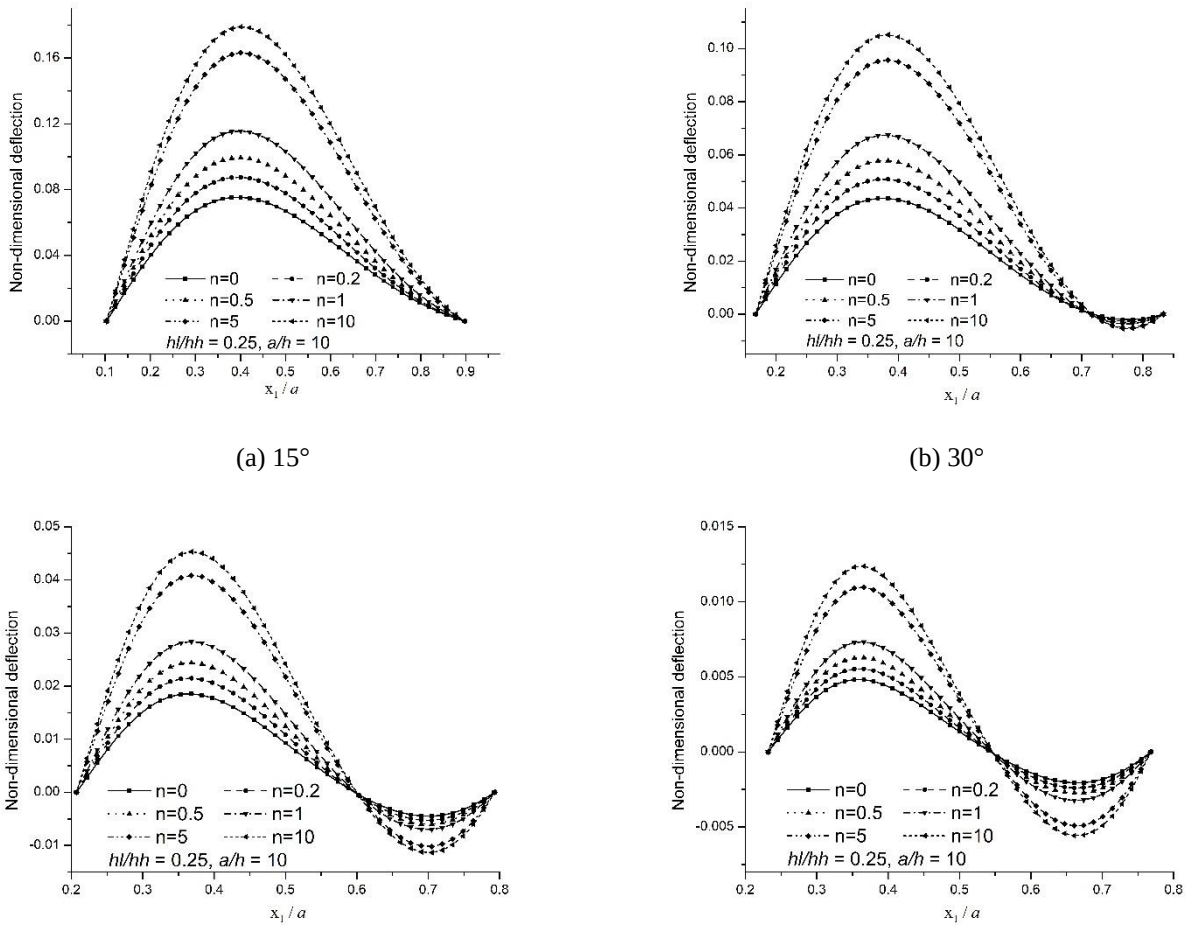

(a) 15°

(b) 30°

(c) 45°

(d) 60°

Fig. 7 Variation of non-dimensional deflection along center line of FGM-2 rhombic 1-8-1 Type-II sandwich conoidal shell for various skew angles subjected to sin-sin load.

6. Conclusion

The bending analysis of FGM sandwich rhombic conoidal shell based on TSDT subjected to the various type of loads using an efficient C^0 FE model is presented. The subsequent outcomes of the present study are written below for the volume fraction indices, skew angles, thickness ratios, *hl/hh* ratios and various types of end support.

- The dimensionless deflection decreases with increase in skew angle.
- Effect of volume fraction on deflection and stresses is more for Type-I (1-0-1) sandwich shell than Type-I (1-2-1) sandwich shell when subjected to a sin-sin load.
- Negative displacement is noticed for skew angle more than 30° subjected to sin-sin loading for both types of sandwich conoidal shell.
- Among the various type of boundary constraints, clamped boundary condition yields the minimum value of dimensionless deflection.
- The dimensionless deflection and dimensionless stresses increase when the thickness of shell increases.
- The non-dimensional deflection and normal stresses at the top of the rhombic shell increase with reduction in *hl/hh* ratio subjected to uniform and sin-sin loading.
- The location of maximum transverse deflection of FGM/FGSM conoidal shell depends on the boundary condition and loading pattern.

References

Abdelaziz, H.H., Atmane, H.A., Mechab, I., Boumia, L., Tounsi, A. and Abbas, A.B.El. (2011), "Static analysis of functionally graded sandwich plates using an efficient and simple refined theory", *Chinese J. Aeronaut.*, **24**(4), 434-448. https://doi.org/10.1016/S1000-9361(11)60051-4

Alashti, R.A. and Khorsand, M. (2011), "Three-dimensional thermo-elastic analysis of a functionally graded cylindrical shell with piezoelectric layers by differential quadrature method", *Int. J. Press. Vessel. Pip.*, **88**(5-7), 167-180. https://doi.org/10.1016/j.ijpvp.2011.06.001

Alipour, M.M. and Shariyat, M. (2017), "Analytical layerwise free vibration analysis of circular / annular composite sandwich plates with auxetic cores", *Int. J. Mech. Mater. Des.*, **13**(1), 125-

157. https://doi.org/ 10.1007/s10999-015-9321-2.

Asemi, K., Salehi, M. and Akhlaghi, M. (2014), "Transient thermal stresses in functionally graded thick truncated cones by graded finite element method", *Int. J. Press. Vessel. Pip.*, **119**, 52-61. https://doi.org/ 10.1016/j.ijpvp.2014.03.002.

Bakshi, K. and Chakravorty, D. (2014), "First ply failure study of thin composite conoidal shells subjected to uniformly distributed load", *Thin-Walled Struct.*, **76**, 1-7. https://doi.org/10.1016/j.tws.2013.10.021.

Bessaim, A., Houari, M.S., Tounsi, A., Mahmoud, S. and Bedia, E.A.A. (2013), "A new higher-order shear and normal deformation theory for the static and free vibration analysis of sandwich plates with functionally graded isotropic face sheets", *J. Sandw. Struct. Mater.*, **15**(6), 671-703. https://doi.org/ 10.1177/1099636213498888.

Civalek, Ö. (2017a), "Buckling analysis of composite panels and shells with different material properties by discrete singular convolution (DSC) method", *Compos. Struct.*, **161**, 93-110. https://doi.org/10.1177/1099636213498888.

Civalek, Ö. (2017b), "Free vibration of carbon nanotubes reinforced (CNTR) and functionally graded shells and plates based on FSDT via discrete singular convolution method", *Compos. Part B*, **111**, 45-49. https://doi.org/10.1016/j.compositesb.2016.11.030.

Dai, H. and Dai, T. (2014), "Analysis for the thermoelastic bending of a functionally graded material cylindrical shell", *Meccanica*, **49**, 1069-1081. https://doi.org/10.1007/s11012-013-9853-1.

Daouadji, T.H. and Adim, B. (2017), "Mechanical behaviour of FGM sandwich plates using a quasi-3D higher order shear and normal deformation theory", *Struct. Eng. Mech.,* **61**(1), 49-63. https://doi.org/10.12989/sem.2017.61.1.049.

Das, A.K. and Bandyopadhyay, J.N. (1993), "Theoretical and experimental studies on conoidal shells", *Comput. Struct.*, **49**(3), 531-536. https://doi.org/10.1016/0045-7949(93)90054-H.

Das, H.S. and Chakravorty, D. (2009), "Composite full conoidal shell roofs under free vibration", *Adv. Vib. Eng.*, **8**(4), 321-328.

Demirbas, M.D. (2017), "Thermal stress analysis of functionally graded plates with temperature-dependent material properties using theory of elasticity", *Compos. Part B,* **131**, 100-124. https://doi.org/10.1016/j.compositesb.2017.08.005.

Demirbas, M.D. and Apalak, M.K. (2017), "Thermal stress analysis of one- and two-dimensional functionally graded plates subjected to in-plane heat fluxes", *Proc. IMechE Part L J. Mater. Design Appl.,* **233**(4), 546-562. https://doi.org/10.1177/1464420716675507.

Dey, A., Bandyopadhyay, J.N. and Sinha, P.K. (1992), "Finite Element Analysis of Laminated Composite Conoidal Shell Structures", *Comput. Struct.*, **43**(3), 469-476. https://doi.org/10.1016/0045-7949(92)90281-4.

Eslami, M.R., Babaei, M.H. and Poultangari, R. (2005), "Thermal and mechanical stresses in a functionally graded thick sphere", *Int. J. Press. Vessel. Pip.*, **82**, 522-527. https://doi.org/10.1016/j.ijpvp.2005.01.002.

Ferreira, A.J.M., Roque, C.M.C., Jorge, R.M.N., Fasshauer, G.E. and Batra, R.C. (2007), "Analysis of Functionally Graded Plates by a Robust Meshless Method", *Mech. Adv. Mater. Struct.*, **14**(8), 577-587. https://doi.org/10.1080/15376490701672732.

Ghannad, M. and Gharooni, H. (2014), "Displacements and stresses in pressurized thick FGM cylinders with exponentially varying properties based on FSDT", *Struct. Eng. Mech.,* **51**(6), 939-953. https://doi.org/10.12989/sem.2014.51.6.939.

Ghosh, B. and Bandyopadhyay, J.N. (1994), "Bending Analysis of Conoidal Shells With cut-outs", *Comput. Struct.*, **53**(1), 9-18. https://doi.org/10.1016/0045-7949(94)90124-4.

Ghosh, G. and Bandyopadhyay, J.N. (1990), "Approximate bending analysis of conoidal shells using the galerkin method", *Comput. Struct.*, **36**(5), 801-805. https://doi.org/10.1016/0045-7949(90)90150-Z.

Hadid, H.A. (1964), "An analytical and experimental investigation into the bending theory of elastic conoidal shell", Ph.D. Dissertation, University of Southampton, England.

Hadji, L., Meziane, M.A.M., Abdelhak, Z., Daouadji, T.H. and Bedia, E.A.A. (2016), "Static and dynamic behavior of FGM plate using a new first shear deformation plate theory", *Struct. Eng. Mech.,* **57**(1), 127-140. https://doi.org/10.12989/sem.2016.57.1.127.

Heydarpour, Y., Aghdam, M.M. and Malekzadeh, P. (2014), "Free vibration analysis of rotating functionally graded carbon nanotube-reinforced composite truncated conical shells", *Compos. Struct.*, **117**(1), 187-200. https://doi.org/10.1016/j.compstruct.2014.06.023.

Jooybar, N., Malekzadeh, P. and Fiouz, A. (2016). "Vibration of functionally graded carbon nanotubes reinforced composite truncated conical panels with elastically restrained against rotation edges in thermal environment," *Compos. Part B Eng.*, **106**, 242-261. https://doi.org/10.1016/j.compositesb.2016.09.030.

Kashtalyan, M. and Menshykova, M. (2009), "Three-dimensional elasticity solution for sandwich panels with a functionally graded core", *Compos. Struct.*, **87**(1), 36-43. https://doi.org/10.1016/j.compstruct.2007.12.003.

Koizumi, M. (1997), "FGM activities in Japan", *Compos. Part B*, **28***B*, 1-4. https://doi.org/10.1016/S1359-8368(96)00016-9.

Kulkarni, S.D., Trivedi C.J. and Ishi R.G. (2015), "Static and free vibration analysis of functionally graded skew plates using a four node quadrilateral element", *Adv. Struct. Eng.*, Springer, New Delhi. https://doi.org/10.1007/978-81-322-2190-6_2.

Kumari, S. and Chakravorty, D. (2010), "Finite element bending behaviour of discretely delaminated composite conoidal shell roofs under concentrated load", *Int. J. Eng. Sci. Technol.*, **2**(4), 54-70.

Malekzadeh Fard, K. and Baghestani, A.M. (2017), "Free vibration analysis of deep doubly curved open shells using the Ritz method", *Aerosp. Sci. Technol.*, **69**, 136-148. https://doi.org/10.1016/j.ast.2017.06.021.

Merdaci, S., Tounsi, A., Houari, M.S.A., Mechab, I., Hebali, H. and Benyoucef, S. (2011), "Two new refined shear displacement models for functionally graded sandwich plates", *Arch. Appl. Mech.*, **81**(11), 1507-1522. https://doi.org/10.1007/s00419-010-0497-5.

Natarajan, S. and Manickam, G. (2012), "Bending and vibration of functionally graded material sandwich plates using an accurate theory", *Finite Elem. Anal. Des.*, **57**, 32-42. https://doi.org/10.1016/j.finel.2012.03.006.

Sayyad, A.S. and Ghugal, Y.M. (2014), "A new shear and normal deformation theory for isotropic, transversely isotropic, laminated composite and sandwich plates", **10**, 247-267. https://doi.org/10.1007/s10999-014-9244-3.

Taj, M.G., Chakrabarti, A. and Talha, M. (2014), "Bending analysis of functionally graded skew sandwich plates with through-the thickness displacement variations", *J. Sandw. Struct. Mater.*, **16**(2), 210-248. https://doi.org/10.1177/1099636213512499.

Tornabene, F. and Viola, E. (2013), "Static analysis of functionally graded doubly-curved shells and panels of revolution", *Meccanica*, **48**, 901-930. https://doi.org/10.1007/s11012-012-9643-1.

Viola, E., Rossetti, L., Fantuzzi, N. and Tornabene, F. (2014), "Static analysis of functionally graded conical shells and panels using the generalized unconstrained third order theory coupled with the stress recovery", *Compos. Struct.*, **112**, 44-65. https://doi.org/10.1016/j.compstruct.2014.01.039.

Xiang, S. and Liu, Y.Q. (2016), "An nth-order shear deformation theory for static analysis of functionally graded sandwich

plates", *J. Sandw. Struct. Mater.*, **18**(5), 579-596. https://doi.org/10.1177/1099636216647928.

Zenkour, A.M. (2013), "Bending analysis of functionally graded sandwich plates using a simple four-unknown shear and normal deformations theory," *J. Sandw. Struct. Mater.*, **15**(6), 629-656. https://doi.org/10.1177/1099636213498886.

Zenkour, A.M. and Alghamdi, N.A. (2008), "Thermoelastic bending analysis of functionally graded sandwich plates", *J. Mater. Sci.*, **43**(8), 2574-2589. https://doi.org/10.1007/s10853-008-2476-6.

Zhao, X., Lee, Y.Y.Ã. and Liew, K.M. (2009), "Thermoelastic and vibration analysis of functionally graded cylindrical shells", *Int. J. Mech. Sci.*, **51**(9-10), 694-707. https://doi.org/10.1016/j.ijmecsci.2009.08.001.

CC